

Effects of crystallization on low-temperature specific heat capacity of $\text{Cu}_{60}\text{Zr}_{20}\text{Hf}_{10}\text{Ti}_{10}$ bulk metallic glass

WANG Zhi-xin, SUN Bin, LU Jin-bin

School of Materials and Chemical Engineering, Zhongyuan Institute of Technology, Zhengzhou 450007, China

Received 17 May 2010; accepted 24 March 2011

Abstract: The specific heat capacities of $\text{Cu}_{60}\text{Zr}_{20}\text{Hf}_{10}\text{Ti}_{10}$ bulk metallic glass (BMG) and crystallized alloys were measured from 2 to 101 K. The effect of crystallization on the specific heat capacity of the BMG was studied. The effects of crystallization and the relationship between local modes and boson peak in the BMG were discussed. The specific heat capacity deviates from the simple Debye behaviors, showing the presence of local harmonic modes (Einstein oscillator) in the BMG and the crystallized alloy. Model calculation includes the contribution of one Debye mode and two Einstein modes for the BMG, one Debye mode and one Einstein mode for the crystallized alloy, showing an adequate description of the experimental data.

Key words: $\text{Cu}_{60}\text{Zr}_{20}\text{Hf}_{10}\text{Ti}_{10}$ BMG; specific heat capacity; crystallization

1 Introduction

The low temperature specific heat capacity is important for understanding the low-energy excitation in bulk metallic glasses (BMGs). At low temperature, typically $T < 1$ K, the specific heat capacity, c_p , of glasses depends approximately linear on temperature [1–3]. At $T > 1$ K, the specific heat capacity deviates from the expected T^3 dependence, presenting a broad maximum in curve of c_p/T^3 [4]. The low temperature specific heat capacity varying linearly with temperature and the anomalous thermal conductivity, was well accounted by the tunneling model [1]. For some BMGs, such as $\text{Zr}_{46.75}\text{Ti}_{8.25}\text{Cu}_{7.5}\text{Ni}_{10}\text{Be}_{27.5}$, $(\text{Cu}_{50}\text{Zr}_{50})_{92}\text{Al}_8$ and $\text{Cu}_{50}\text{Zr}_{50}$, their low temperature specific heat capacities were well fitted by the Debye mode and the Einstein mode [5–8]. The thermal properties of alloys directly related to its atomic structure, or its vibrational and configurational entropy which is significantly affected by the nearest-neighbor configuration [8–9]. BMGs are usually metastable at room temperature and will form crystalline or quasicrystalline phases when the temperature increases to the phase transition temperature [10–12]. Crystallization of BMGs makes changes in structure and physical properties [13–14]. Amorphous solids exhibit unusual thermal properties at low temperature, which are

in turn very different from those of crystalline solids [1]. Recently, some works have shown the low temperature thermal properties of the Zr-, Cu-, and La-based BMGs, and the effects of composition or heat treatment (no crystallization) on the low temperature specific heat capacity of the BMGs [6, 8, 15]. However, there is little information about effects of crystallization on the low-temperature specific heat capacity of BMGs. In this work, we report the observation of $\text{Cu}_{60}\text{Zr}_{20}\text{Hf}_{10}\text{Ti}_{10}$ BMG which has excellent glass-forming ability and mechanical properties [16] and the crystallized alloys by measuring the specific heat capacity from 2 to 101 K. The effect of crystallization on the low-temperature specific heat capacity of $\text{Cu}_{60}\text{Zr}_{20}\text{Hf}_{10}\text{Ti}_{10}$ BMG was discussed.

2 Experimental

$\text{Cu}_{60}\text{Zr}_{20}\text{Hf}_{10}\text{Ti}_{10}$ BMG was prepared by melting highly pure elements and by suction casting the melt into a copper mold under pure argon atmosphere. The glass transition temperature T_g , onset crystallization temperature T_x , and the melting temperature T_m of the $\text{Cu}_{60}\text{Zr}_{20}\text{Hf}_{10}\text{Ti}_{10}$ BMG are 734, 782, and 1 189 K, respectively [17]. The crystallized alloy was got by annealing the BMG at 873 K for 2 h. The structure of the samples was identified to be amorphous by X-ray

diffraction (XRD) and differential scanning calorimeter (DSC). Specific heat capacity measurements were carried out between 2 and 101 K with the heat capacity option of the commercial physical property measurement system (PPMS, Quantum Design, USA). According to the specifications, the relative error on the specific heat capacity measurements on this instrument is less than 2%. The masses of the samples of the $\text{Cu}_{60}\text{Zr}_{20}\text{Hf}_{10}\text{Ti}_{10}$ BMG and crystallized alloys, which are used for the measurements, were 15.19 and 13.46 mg, respectively.

3 Results and discussion

3.1 Structure of $\text{Cu}_{60}\text{Zr}_{20}\text{Hf}_{10}\text{Ti}_{10}$ BMG at different states

Figure 1 shows the XRD patterns of the $\text{Cu}_{60}\text{Zr}_{20}\text{Hf}_{10}\text{Ti}_{10}$ BMG at different states. The XRD pattern of the as-cast alloy shows a broad diffused peak without any detectable crystallized peaks, indicating a glass structure within the examining limit of the XRD. After being annealed at 873 K for 2 h, the BMG contains Cu_8Zr_3 , $\text{Cu}_{10}\text{Zr}_7$ and some unknown crystalline phases, as shown in Fig. 1.

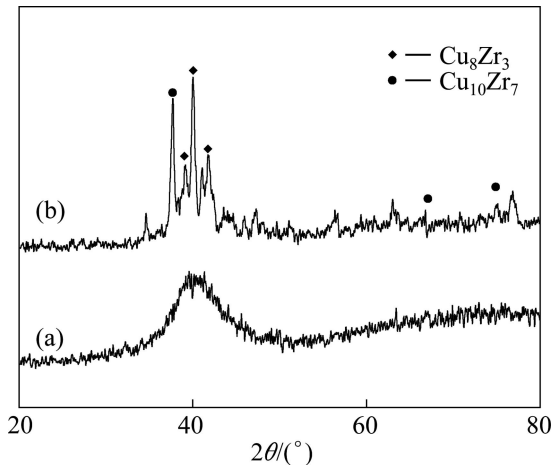


Fig. 1 XRD patterns of $\text{Cu}_{60}\text{Zr}_{20}\text{Hf}_{10}\text{Ti}_{10}$ BMG at different states: (a) As-cast; (b) Annealed at 873 K for 2 h

Figure 2 shows the DSC traces of $\text{Cu}_{60}\text{Zr}_{20}\text{Hf}_{10}\text{Ti}_{10}$ BMG at different states. The DSC trace of the as-cast alloy shows crystallization process (exothermic). No exothermic process occurs in DSC measurement of the annealed sample, indicating that crystallization of $\text{Cu}_{60}\text{Zr}_{20}\text{Hf}_{10}\text{Ti}_{10}$ BMG is finished completely after being annealed.

3.2 Low-temperature specific heat capacity of samples at different states

The measured specific heat capacities of the $\text{Cu}_{60}\text{Zr}_{20}\text{Hf}_{10}\text{Ti}_{10}$ BMG and the crystallized alloy from 2 K to 101 K are shown in Fig. 3. It can be clearly seen

that the temperature-dependent specific heat capacity is different for the two alloys. The BMG has larger specific heat capacity than the crystallized alloy, just like other alloys [18]. Figure 3(b) shows the specific heat capacity

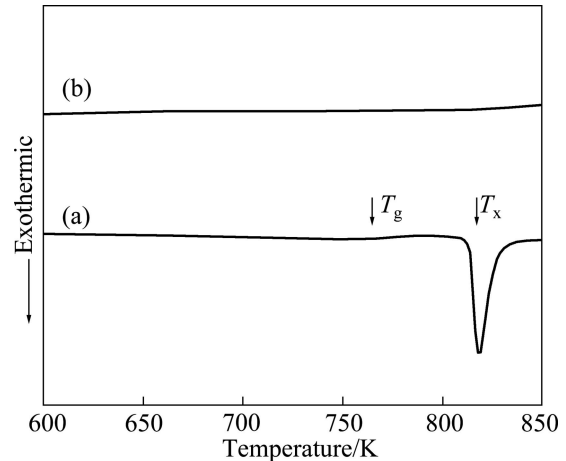


Fig. 2 DSC traces of $\text{Cu}_{60}\text{Zr}_{20}\text{Hf}_{10}\text{Ti}_{10}$ BMG at different states: (a) As-cast; (b) Annealed at 873 K for 2 h

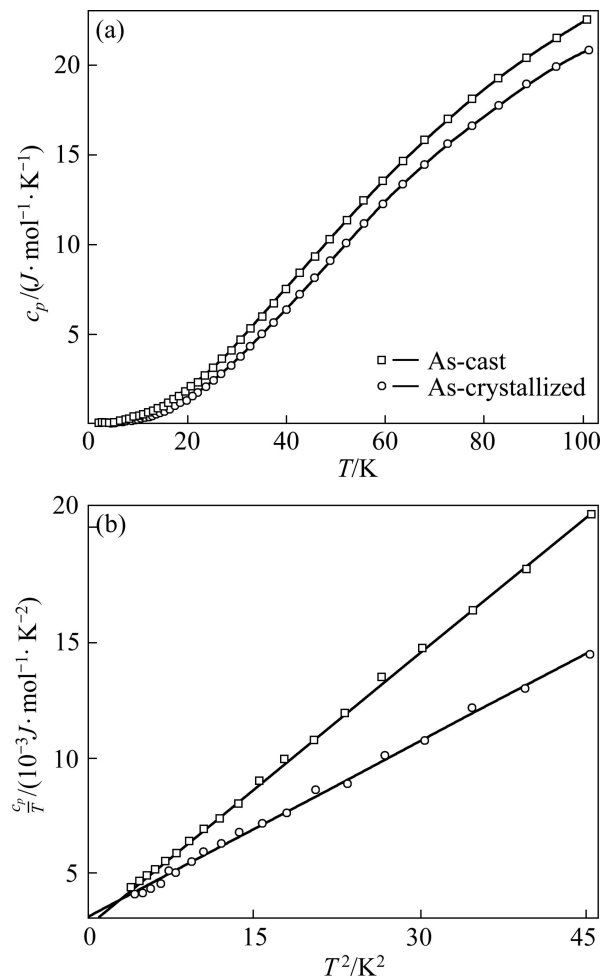


Fig. 3 Specific heat capacity c_p of $\text{Cu}_{60}\text{Zr}_{20}\text{Hf}_{10}\text{Ti}_{10}$ BMG at different states in temperature range from 2 to 101 K (a), and fitting of specific heat capacity of BMG and crystallized alloy between 2–6.7 K using expression $c_p/T = \gamma + \beta T^2$ (b)

in the temperature range of 2–6.7 K, which is analyzed for both alloys by fitting with a polynomial form:

$$c_p/T = \gamma + \beta T^2 \quad (1)$$

where γ is coefficient of temperature T for the electron contribution to the specific heat, and β is the coefficient of T^3 for the phonon contribution to the specific heat. So we can get that γ is 2.73 mJ/(mol·K²) for the BMG and 3.15 mJ/(mol·K²) for the crystallized alloy.

The low-temperature specific heat capacity of the BMGs could change with the heat treating. The height of peak in c_p of (Cu₅₀Zr₅₀)₉₂Al₈ BMG decrease during the annealing process (no crystallization occurred) [6]. The peak height of the low-temperature c_p of Zr_{46.75}Ti_{8.25}Cu_{7.5}Ni₁₀Be_{27.5} BMG decreased in the quenched process (the quenched temperature was less than the glass transition temperature, and no crystallization occurred in quenched process) [6]. The values of γ and β for the BMGs at different states were compared and listed in Table 1.

3.3 Atom state contribution to specific heat capacity for different samples

The c_p of an elastic continuum normally can be explained by the Debye model in a wide temperature range. We found that the specific heat capacity of Cu₆₀Zr₂₀Hf₁₀Ti₁₀ BMG and the crystallized alloy cannot be well fitted only by the Debye mode and the electron contributions and an additional of Einstein mode is required to fit c_p adequately. As illustrated in Fig. 4, a model calculation includes the contribution of one Debye mode and two Einstein modes for the BMG, one Debye mode and one Einstein mode for the crystalline alloy, respectively, showing an adequate description of the experimental data. The line through the specific heat capacity data in Fig. 4 represents a fitting to the equation:

$$c_p = \gamma T + n_D C_D + \sum_{i=1}^m n_{Ei} C_{Ei} \quad (2)$$

where n_D and n_{Ei} are constants, just the oscillator strengths per mole at different energies; T is temperature; C_D represents contribution from Debye mode.

$$C_D = 3R \left(\frac{T}{\theta_D}\right)^3 \int_0^{\theta_D/T} \frac{\xi^4 e^\xi}{(e^\xi - 1)^2} d\xi \quad (3)$$

where R is the gas constant and θ_D is the Debye temperature; C_E is the contribution from Einstein mode.

$$C_E = R \left(\frac{\theta_E}{T}\right)^2 \frac{e^{\theta_E/T}}{(e^{\theta_E/T} - 1)^2} \quad (4)$$

where θ_E is the Einstein temperature. All fitting parameters are summarized in Table 2. The strength of Einstein modes in the BMG is higher than that in the crystallized alloy.

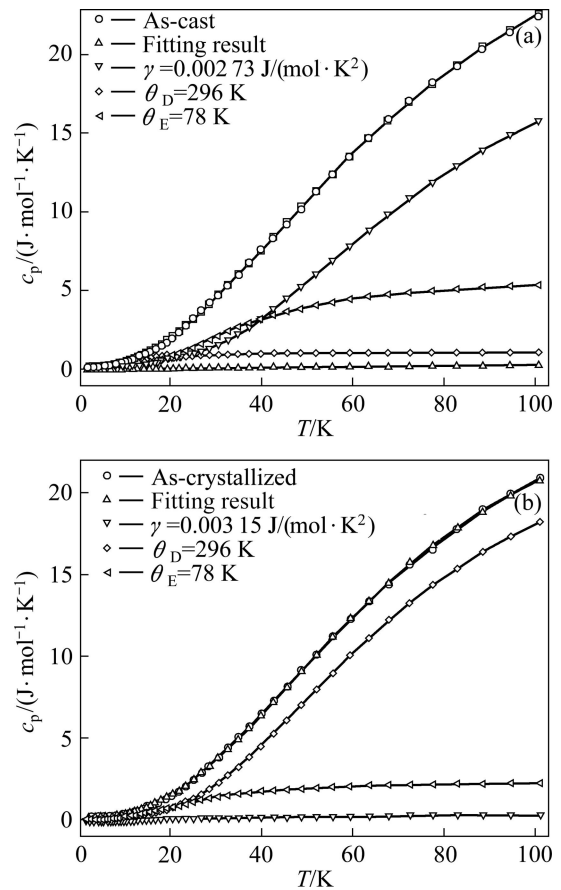


Fig. 4 Fitting results of Cu₆₀Zr₂₀Hf₁₀Ti₁₀ BMG at different states between 2 K and 101 K: (a) As-cast; (b) As-crystallized

Table 1 Values of γ and β for BMGs at different states

Sample	State	γ /(mJ·mol ⁻¹ ·K ⁻²)	β /(mJ·mol ⁻¹ ·K ⁻⁴)
Cu ₆₀ Zr ₂₀ Hf ₁₀ Ti ₁₀	As-cast	2.73	0.39
	As-crystallized	3.15	0.25
(Cu ₅₀ Zr ₅₀) ₉₂ Al ₈ [15]	As-cast	3.06	0.17
	Annealed at 673 K for 1 h	2.97	0.1
Zr _{46.75} Ti _{8.25} Cu _{7.5} Ni ₁₀ Be _{27.5} [15]	As-cast	3.36	0.11
	Cooling rate of 40 K/min from 713K	3.47	0.1

Table 2 Fitting parameters

Sample state	Mode	$\theta_D, \theta_E/K$	n
As-cast	D	331	3.08
	E1	41	0.13
	E2	113	0.72
As-crystallized	D	296	3.25
	E	78	0.28

E, E1 and E2 are Einstein modes; D is Debye mode; n is oscillator per mole

Usually, local harmonic modes are difficultly found by measuring the specific heat capacity because of the strong interaction between the constituent atoms. But when BMGs are quickly quenched from liquid state, the icosahedral structure or large hole is kept in BMGs. There is much free volume in the oversized cage structure. There is the difference of the density between BMGs and corresponding crystalline alloys [13]. The vibrations of the loose atoms with enough large free volume are as independent local modes. So the independent local mode in the BMG shows Einstein modes by fitting of the specific heat capacity. After the BMG being crystallized, the free volume is reduced and the strength of Einstein modes is also decreased.

3.4 Boson peak in $\text{Cu}_{60}\text{Zr}_{20}\text{Hf}_{10}\text{Ti}_{10}$ BMG

The unusual phenomena in amorphous solids are phonon-like excitations, which exist at very high frequency (10^{12} Hz), and the related vibrational density of states. A universal feature of such amorphous systems is that the vibrational density of states departs from the Debye squared-frequency law, displaying an excess state, which has been named the Boson peak. The feature was mainly observed in polymeric and ceramic glasses before. In the BMG and crystallized alloys, the three-dimensional spectra are derived from the specific heat. We supposed the phonon density of states contributed from the Einstein mode is in Gaussian distribution [19]:

$$n_E(T) = \frac{n_E}{\sigma\sqrt{2\pi}} \exp\left[-\frac{(T-\theta_E)^2}{2\sigma^2}\right] \quad (5)$$

where σ is the width of Gaussian ($\sigma=\theta_E/3$). The derived three-dimensional phonon spectra of both BMG and crystallized alloys are greatly different. There is higher density of states at low energy in the BMG than in crystallized alloy. So just like many other amorphous alloys [20], the excess density of states in the BMG is just reduced by the Boson peak.

There are many methods by experiments to definite boson peak, such as a peak in Raman scattering data [21], a peak in the neutron scattering data [20], a peak in the

difference between the vibrational density of states of the glass and the corresponding crystal [20]. We select the third method to determine the boson peak, which is shown in Fig. 5(a). Figure 5(b) presents the total density of states of the amorphous and crystallized alloys.

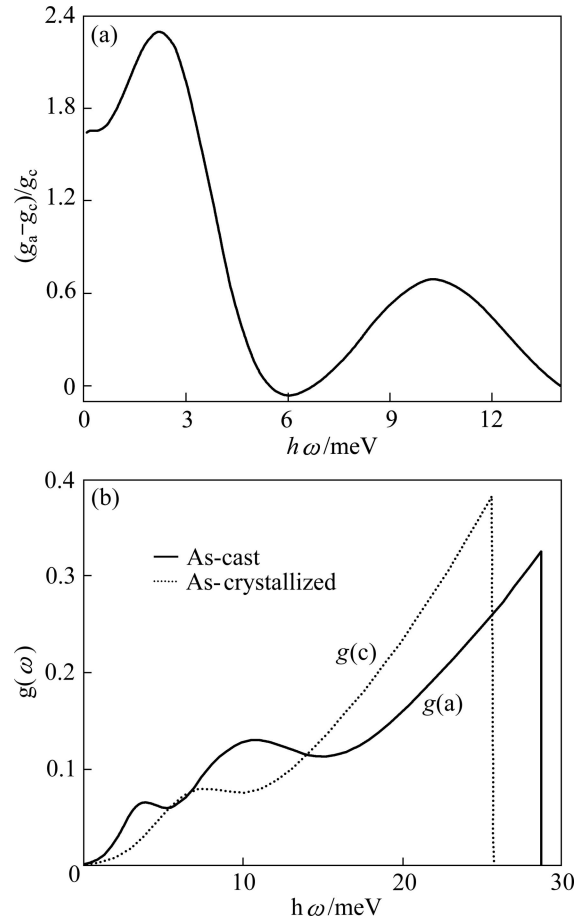


Fig. 5 Rate between derived three-dimensional phonon spectrums of $\text{Cu}_{60}\text{Zr}_{20}\text{Hf}_{10}\text{Ti}_{10}$ BMG at different states (a) and total three-dimensional phonon spectrum of both alloys (b) (g_a and g_c represent total density of states of glass state and crystallized state, respectively)

4 Conclusions

1) The temperature-dependent specific heat capacity of the $\text{Cu}_{60}\text{Zr}_{20}\text{Hf}_{10}\text{Ti}_{10}$ BMG is affected by crystallization and the specific heat capacity of the BMG decreases after being crystallized.

2) The specific heat capacity of the BMG and the crystallized alloy deviate from the simple Debye behaviors. Two additional Einstein modes for the BMG and one Einstein mode for the crystallized alloy are required to fit the c_p results adequately.

3) The three-dimensional spectrums derived from the specific heat capacity shows boson peak in the BMG, which is associated with local harmonic modes.

References

- [1] ZELLER R C, POHL R Q. Thermal conductivity and specific heat of noncrystalline solids[J]. *Phys Rev B*, 1971, 4: 2029–2041.
- [2] ANDERSON P W, HALPERIN B I, VARMA C M. Anomalous low-temperature thermal properties of glasses and spin glasses[J]. *Philos Mag*, 1972, 25: 1–9.
- [3] PHOLLIPS W A. Tunneling states in amorphous solids[J]. *J Low Temp Phys*, 1972: 351–360.
- [4] GIL L, RAMOS M A, BRING A, BUCHENAU U. Low-temperature specific heat and thermal conductivity of glasses[J]. *Phys Rev Lett*, 1993, 70(1–4): 182.
- [5] TANG M B, BAI H Y, PAN M X, ZHAO D Q, WANG W H. Einstein oscillator in highly-random-packed bulk metallic glass[J]. *Appl Phys Lett*, 2005, 86(1–3): 021910.
- [6] LI Y, YU P, BAI H Y. Study on boson peak in bulk metallic glasses[J]. *J Appl Phys*, 2008, 104(1–7): 013520.
- [7] LI Y, BAI H Y, WANG W H. Low-temperature specific-heat anomalies associated with the boson peak in CuZr-based bulk metallic glasses[J]. *Phys Rev B*, 2006, 74(1–4): 052201.
- [8] TANG M B, BAI H Y, WANG W H. Tunneling states and localized mode in binary bulk metallic glass[J]. *Phys Rev B*, 2005, 72(1–4): 012202.
- [9] ALEINER I L, ALTSHULER B L, GALPERIN Y M. Experimental tests for the relevance of two-level systems for electron dephasing[J]. *Phys Rev B*, 2001, 63(1–4): 201401.
- [10] LOUZGUINE-LUZGIN D V, ANTONOWICZ J, GEORGARAKIS K, VAUGHAN G, YAVARI A R, INOUE A. Real-space structural studies of Cu-Zr-Ti glassy alloy[J]. *J Alloys Compd*, 2008, 466: 106–110.
- [11] WANIUK T, SCHROERS J, JOHNSON W L. Timescales of crystallization and viscous flow of the bulk glass-forming Zr-Ti-Ni-Cu-Be alloys[J]. *Phys Rev B*, 2003, 67(1–6): 184203.
- [12] XIA L, DING D, SHAN S T, DONG Y D. Evaluation of the thermal stability of Nd₆₀Al₂₀Co₂₀ bulk metallic glass[J]. *Appl Phys Lett*, 2007, 90(1–4): 111903.
- [13] WANG Z X, WANG R J, WANG W H. Elastic properties of Cu₆₀Zr₂₀Hf₁₀Ti₁₀ bulk metallic glass under high pressure[J]. *Materials Letters*, 2006, 60: 831–833.
- [14] SCHROERS J, WU Y, BUSH R, JOHNSON W L. Transition from nucleation controlled to growth controlled crystallization in Pd₄₃Ni₁₀Cu₂₇P₁₀ melts[J]. *Acta Mater*, 2001, 49: 2773–2781.
- [15] TANG M B, BAI H Y, PAN M X, ZHAO D Q, WANG W H. Bulk metallic superconductive La₆₀Cu₂₀Ni₁₀Al₁₀ glass[J]. *J Non-crystalline Solids*, 2005, 351: 2572–2575.
- [16] INOUE A, ZHANG W, ZHANG T, KUROSAKA K. Cu-based bulk glassy alloy with good mechanical properties in Cu-Zr-Hf-Ti system[J]. *Mater Trans JIM*, 2001, 42: 1805–1812.
- [17] WANG Z X, LU J B, XI Y J. Effects of quenched under high pressure on crystallization of Cu₆₀Zr₂₀Hf₁₀Ti₁₀ bulk metallic glass[J]. *Mater Sci Eng A*, 2009, 499: 192–194.
- [18] BAI H Y, LUO J L, ZHANG J, CHEN Z J. Low temperature specific heat of a typical glass forming alloy[J]. *J Appl Phys*, 2002, 91: 9123–9127.
- [19] HERMANN R P, JIN R Y, SCHWEIKA W, GRANDJEAN F, MANDRUS D, SALES B C, LONG G J. Einstein oscillators in thallium filled antimony skutterudites[J]. *Phys Rev Lett*, 2003, 90(1–4): 135505.
- [20] MEYER A, WUTTKE J, PETRY W, PEKER A, BORMANN R, CODDENS G, KRANICH L, RANDL O G, SCHOBER H. Harmonic behavior of metallic glasses up to the metastable melt[J]. *Phys Rev B*, 1996, 53: 12107–12111.
- [21] SOKOLOV A P, KISLIUK A, SOLTWISCH M, QUITMANN D. Medium-range order in glasses: Comparison of Raman and diffraction measurements[J]. *Phys Rev Lett*, 1992, 69: 1540–1543.

晶化过程对 Cu₆₀Zr₂₀Hf₁₀Ti₁₀ 块体金属玻璃低温比热容的影响

王志新, 孙斌, 卢金斌

中原工学院 材料与化工学院, 郑州 450007

摘要: 测量 Cu₆₀Zr₂₀Hf₁₀Ti₁₀ 块体金属玻璃和其晶化态合金在 2~101 K 的比热, 研究晶化过程对块体金属玻璃比热的影响。讨论晶化过程对 Cu₆₀Zr₂₀Hf₁₀Ti₁₀ 块体金属玻璃低温比热和块体金属玻璃的波色峰的影响。结果表明: 这两种合金的比热都与单一的德拜模型不相符, 都存在着局域谐振模型(爱因斯坦模型)。分别用一个德拜模型和两个爱因斯坦模型拟合玻璃态合金, 用一个德拜模型和一个爱因斯坦模型拟合晶化态合金, 拟合结果与实验数据吻合得很好。

关键词: Cu₆₀Zr₂₀Hf₁₀Ti₁₀ 块体金属玻璃; 比热; 晶化

(Edited by LI Xiang-qun)